Effect of Powder Characteristics on Flash Sintering of Hydroxyapatite

Kiran S. Naik[a], Pradnyesh P. Satardekar[b], John. A. Downs[c], Vincenzo M. Sglavo[c]

[a]*Department of Chemistry, PES's Ravi S. Naik College of Arts and Science, Ponda, Goa, India*
[b]*Department of Chemistry, HPSM's Ganpat Parsekar College of Education, Harmal, Goa, India*
[c]*Department of Industrial Engineering, University of Trento, Trento, Italy*

Abstract

A comparative study on flash sintering of hydroxyapatite (HA) with two different powder characteristics is presented in this work. Electric fields up to 2000 V cm^{-1} were tested, resulting in sintering at temperatures as low as 850°C and density in excess to~~ies ->~~90%. XRD and FTIR analysis show no decomposition of HA into other phases for conventional as well as for flash sintering. In general, the conductivity curve for HA is found to be different from that of other materials~~,~~ and this is attributed to the microstructural changes taking place due to the dehydroxylation reaction ~~happening~~ occurring during sintering. Powder characteristics are shown to influence the conductivity curve and also the onset temperature for flash, although the overall character of the curve remains similar. Sintering conditions that lead to the partial melting of the samples exhibit (002) preferred oriented microstructure.

Key words

Flash sintering, Hydroxyapatite, Powder characteristics, Biomaterial

Introduction

Hydroxyapatite (HA) is a commonly used bio-ceramic because of its chemical and structural similarities with bone tissue resulting in superior biocompatibility [1] [2] [3] [4]. HA is typically produced as a powder that is formed by many different ceramic processing techniques into a low density, low strength 'green' body which is then densified by heat treatment. To obtain a high degree of densification and high mechanical strength, the material must be subjected to high temperature, typically over 1200°C. Such a sintering process improves the mechanical properties but can activate other processes resulting in grain growth, phase separation and decomposition [5].

To enhance densification and ~~the~~ mechanical properties ~~and densification~~ of HA, several sintering techniques have been ~~studied~~investigated. The addition of small amounts of a low melting sintering aids increases diffusion rates and improves ~~the~~ sinterability of HA [6]. Other sintering methods such as hot pressing (HP) [7] [8] and hot isostatic pressing (HIP) [9] deployed to enhance the densification of HA use externally applied pressure and thermal energy. Other approaches, known as Field Assisted Sintering Techniques (FAST), use electromagnetic fields or microwaves to enhance diffusion rates [9] [10]. Microwave sintered HA possesses ~~a~~ higher density and exhibits much lower grain growth compared to ~~the one~~the material sintered conventionally. HA has also been sintered at lower temperature by spark plasma sintering (SPS) where electric field, thermal energy and pressure are combined [11].

The seminal work of Cologna *et.al* [10] identified a new FAST technique called "~~f~~Flash sintering" where ~~sintering~~ densification occurs by ~~just applying~~the application of a DC electric field in combination with a (limited) thermal energy ~~of~~ from the furnace. The technique was shown to cause sintering of ceramics in less than 5 seconds and at a much lower temperature than in conventional sintering. The mechanisms remain mostly unclear at present, but Joule heating and high defects concentration are predicted as the fundamental causes for such an effective diffusion rate [11]. Flash sintering technique have been studied on several materials [10] [12] [13] [14] [15] [16], including HA [17] [18] [19]. Overall, the sintering temperature and processing time were shown to reduce ~~effectively~~substantiallu~~,~~ and the phase transformation was minimized for ~~the~~ HA densified by flash sintering.

Powder characteristics have been shown to considerably influence the flash phenomena on 3 mol% yttria-stabilized zirconia [20], and therefore it is worth studying the effect of powder characteristics on flash sintering of HA. In this work, we present a study on flash sintering phenomena at different applied E-fields on two HA powders with different powder characteristics.

Materials and Methods

Two commercially available HA powders were used in the present work. One is a spray-dried powder (Fluidinova, S.A., Engenharia de Fluidos, Portugal), here on called HA-A. The other is an agglomerated powder (Eurocoating, Italy), here on called HA-B. Each powder was mixed

Formattato: Rientro: Prima riga: 1,27 cm

with 3 wt% polyacrylate binder (Duramax B-1000, Rohm and Haas France SAS, BP, France) and uniaxially pressed into dog-bone shaped pallets similar to those shown in [21] [22]. ~~Pressing~~ Uniaxial pressing with 120 MPa within a steel mould (REF) resulted in an initial relative green density of~44% (theoretical density for HA = 3.16 g cm^{-3}) which was obtained from dimensional parameters and ~~weight~~ mass of the sample. The effective dimensions of the rectangular section of the dog bone specimen were 21 mm between the electrodes x 3 mm width x 1.80 ± 0.03 mm thickness.

The field-assisted sintering setup and procedure were similar to those described in [22]. The sample was suspended in the hot zone of a sealed horizontal tubular furnace (HTRH 100-300/18, GERO Hochtemperaturöfen GmbH, Germany) by two platinum wires (diameter = 0.5 mm) run through the holes in the handles of the dog bone specimen. The electrodes served to hold the sample freely and to apply the necessary voltages and required currents. The sample shrinkage was monitored by a CCD camera through a silica window at one end of the alumina tube. The furnace temperature was monitored by an S-type thermocouple kept in the hot zone of the furnace, at about 10 mm from the sample, to minimize the error due to Joule heating of sample ~~resulting from the Joule heating~~ [11]. Artificial dry air was fluxed through the furnace chamber for the duration of each experiment to minimize arcing issues and to maintain a dry atmosphere. All treatments were carried out with a constant heating rate of 10°C min^{-1} up to 1400°C or until a flash sintering event occurred. After sintering, the density was determined by the Archimedes' method.

Experiments were carried out with and without the application of an electric field (E-field). The required voltage (V) to achieve the desired E-field (E) based on the initial electrode separation (L_0 = 21 mm) and determined as $E=V/L_0$, was applied at 600°C after complete burnout of the binder ~~from the samples~~. ~~Voltage~~ The voltage was maintained constant throughout the sintering treatment. The current was monitored by a digital multimeter and current density (J) was determined based on the initial sample cross-section (J=I/(thickness x width)). The volumetric power dissipation was calculated as the product of E-field and current density (P=E x J). When the current density abruptly increased in the "flashing" dog-bone sample, the power supply and furnace were turned off and the sample was allowed to cool at the furnace rate.

The morphology of starting powder and microstructure~~s~~ of sintered samples were examined by SEM (JEOL JSM-5500E). The particle size distribution of the powders was

Formattato: Rientro: Prima riga: 1,27 cm

obtained from the analysis of SEM images using Image J software. Crystalline phases were analyszed before and after sintering by XRD (Rigaku DMax - Bragg-Brentano configuration). The samples were exposed to Cu K-α radiation with steps of 0.02°, ~~with~~ hold time of 6 s at each scan of 2 theta from 20° to 55°. Fourier Transformation Infra-Rred (FTIR) spectrometry was used to compare the dehydration of HA before and after sintering (Nicolet Avatar 330, Thermo Electo Corporation, Waltham, MA.); crushed samples were mixed with KBr and scanned at an average rate of 64 scans s^{-1} with 4 cm^{-1} resolution.

Results and Discussion

Powder Properties~~:~~

Formattato: Sottolineato

The morphology of ~~two~~ HA powders are shown in figure 1. HA-A powder has a spherical morphology, whereas HA-B powder consists of hard agglomerates which are irregular in shape. Figure 2 shows the particle size distribution for the two powders. HA-A has a narrower ~~particle~~ size distribution with an average particle size of 1.33 µm (standard deviation = 0.47 µm)~~;~~, HA-B on other hand ~~has~~ is characterized by a wider particle size distribution with an average particle size of 2.39 µm (standard deviation = 1.11 µm).

Sintering~~:~~

Formattato: Sottolineato

Shrinkage strain as a function of furnace temperature at different applied E-fields for the HA compacts is shown in figure 3. For conventional sintering, it can be seen that the two powders show different sintering behaviors. ~~Dependence~~ The dependence of sintering behavior (for conventional sintering) of HA on powder morphology has been already shown in previous works [23] [24]. HA-A shows better sinterability ~~for~~ upon conventional sintering with a final shrinkage strain of ~~-~~24.8 % in comparison to HA-B ~~with~~ characterized by a final shrinkage strain of 23.1 %, as ~~, this is~~ reflected ~~in~~ by the~~ir~~ final density reported in table 1. The characteristics of the powders used in this study are comparable to ~~the ones~~those studied in [23]. It was shown that ~~the~~ HA powder with spherical morphology, smaller particle size and a narrower size distribution ended up with higher final density when sintered conventionally at 1400°C, ~~this is~~ in agreement with the current study.

In the presence of an applied E- field, the sintering process occurs at a faster rate. The onset of sintering is shifted to ~~a~~ lower temperature with the applied E-field for compacts of both ~~the~~ powder~~s types~~. ~~For the applied~~Under an E-field of 500 V cm^{-1}, although the sintering rate increases, the character of the sintering curve is similar to ~~that of~~the conventional ~~sintering~~ one for both ~~the~~ powder morphologies. For HA-B, the extremely high sintering rate (wherein the densification occurs within seconds) is observed for the applied E-field of 1500 V cm^{-1} and above~~,~~, however, for HA-A, such extremely high sintering rate is observed only at ~~the~~ applied E-field of 2000 V cm^{-1}.

Table 1 shows the final density of all ~~the~~ sintered samples. It should be noted that the variation in densities for samples sintered in the presence of applied E-field is likely a result of the uncontrolled finishing conditions. The final density is a function of the final current densit~~y~~ies and the time for which the sample is kept in the flash sintering conditions [25]. In our case, these conditions were not controlled; therefore, even a few seconds more in flash conditions even at lower applied E-field can result in higher densities due to the extremely high diffusion rate.

Microstructure~~:~~

Formattato: Sottolineato

The ~~micrographs of a~~ fractured surface of sintered samples ~~are~~ is shown in figure 4. It can be seen that a nearly dense microstructure with few pores and grains in the micron range is obtained for all the samples regardless ~~of~~ the powder type and the applied E-field. ~~However~~Nevertheless, HA-A sintered at an applied E-field of 500 V cm^{-1} shows a unique microstructure that is different from ~~the rest of~~ the other flash sintered samples. The unique nature of the microstructure could be very likely ~~because~~ accounted for by ~~of~~ partial melting, ~~this~~ at ~~is~~ discussed in more detail in ~~the further~~a following section ~~of~~ (XRD analysis). Again, the variations in microstructure for sintering at different applied E-field can be attributed to the uncontrolled finishing conditions, as previously discussed ~~earlier~~.

Power / electrical conduction~~:~~

Formattato: Sottolineato

Formattato: Rientro: Prima riga: 0 cm

Figure 5 shows the power density curves plotted in Arrhenius format for flash sintered HA sample from 700°C onwards. The power curves ~~in flash sintering studies of~~for HA flash sintering are different from ~~the ones~~those recorded on~~of~~ other materials [17]. In the present study, two different types of power curves are ~~seen~~observed. For the samples

sintered ~~with~~ under high ~~applied~~ E-field (for HA-A sintered ~~with~~ under 2000 V cm^{-1} and for HA-B sintered ~~with~~ under 2000 V cm^{-1} and ~~-~~1500 V cm^{-1}), there is a constant ~~rise~~ increase in conductivity along with the heating process, followed by a sudden conductivity ~~increase~~ intensification ~~in conductivity at a point~~ where the flash event occurs. For ~~the rest of the~~the other combinations of HA powder ~~type~~ and applied E-field the conductivity increases with the thermal process, ~~however~~although, the curves show a 'wavy' nature beginning from~850^{o}C, ~~which is then~~ followed by ~~the~~ a sudden conductivity increase ~~in conductivity~~ leading to the flash event.

Power density plots in Arrhenius-like diagram ~~format for the two powder types~~ at the same applied E-fields are shown for the two powders in figure 6. It can be seen that the temperature for the flash onset ~~of flash~~ is lower for HA-B for the same applied E-field, except for 2000 V cm^{-1}~~;~~ ~~(this is represented in~~ figure 7~~)~~. The fact that the power density plot does not coincide for the two powders (although the character of the curves is similar), infers that the conductivity ~~observed~~ is not only dependent on the intrinsic resistance of the material but relies also ~~depends~~ on the compact resistance ~~of the compact~~ [20]. In ~~the sense that~~other words, powders with different ~~powder~~ characteristics ~~will be~~are packed differently in the green ~~sample~~ component, this leading to different electrical resistance. Initially, at low temperatures, the compacts of HA-B ~~have~~ are more ~~resistance~~resistive. We speculate that the ~~powder characteristics~~ HA-B powder is such that, as the temperature increases and ~~as~~ the sintering process ~~continues resulting in a~~induces changes in the microstructure, the resistance of the HA-B compacts ~~of HA-B~~ decreases. As a result of this resistance decrease ~~in resistance~~, the conductivity of HA-B increases (the 'wavy' nature begins) and exceeds that of HA-A at the particular temperature~~, that is,~~and a crossover takes place as ~~can be seen~~shown in figure 6. The temperature at which the cross-over takes place ~~is seen to~~ decreases with ~~the increasing~~the applied E-field, this being probably related to faster ~~which could be because~~ sintering ~~is faster~~ at higher applied E-field which induces quicker ~~, the higher degree of sintering means the~~ microstructural changes ~~will take place faster~~. ~~This~~ Said crossover causes the temperature for the onset of flash to be lower for HA-B for the same applied E-field. ~~For the applied E-field of~~At 2000 V cm^{-1}, the flash for HA-A occurs at such a low temperature that the crossover does not take place.

From the analysis of figures 5 and ~~figure~~ 6~~,~~ and from the above discussion the following points ~~in view of flash sintering of HA~~ can be inferred: 1) ~~Regardless~~ regardless of the powder

type and the applied E-field, all the power curves ~~would~~ have a similar character (constant increase in conductivity followed by 'wavy' nature) if the flash event had not to occur, 2) ~~The~~ the resistance of the compact influences the power curve, although the character of the curve remains similar, 3) ~~The~~ the powder characteristics play an important role in ~~deciding~~ determining the temperature for the flash onset ~~of flash~~.

Thermal runaway and the generation and ~~movement of~~ defects formation/diffusion in the material are typically considered as the main reasons for the occurrence of flash event. ~~With the increase in~~As temperature rises, the defects concentration also increases~~,~~ and, when the defects concentration exceeds ~~the~~ a threshold value, the current flows through the material, ~~which causes~~this causing the generation of heat ~~inside~~ within the sample. The further increase in temperature due to the generated heat ~~generated~~ further increases the defects concentration, resulting in a synergistic effect of increasing heat ~~generation~~production. Such a chain reaction causes the flash event [25] [18]. For HA, the ~~major~~ fundamental defects which contribute to electrical conduction are hydroxide (OH^-) and hydrogen ~~ions~~ (H^+) ions [26] [27] [28] [29]. The dehydroxylation reaction occurring at high temperatures (at 800°C or above) [30] in HA is considered to be the source for the generation of ~~these~~ such defects [26]. ~~This~~ Such dehydroxylation reaction can ~~be given as~~expressed as:

$$Ca_{10}(PO_4)_6(OH)_2 \rightarrow Ca_{10}(PO_4)_6(OH)_{2-2x}O_x(\square)_x + xH_2O_{(g)} \uparrow \qquad (1)$$

~~Where~~ where $x<1$ and (□) is the vacancies at the hydroxyl site. From Eq~~uation~~ 1, ~~follows that for~~ every two moles of released H_2O ~~released~~, one mole of H^+ ~~vacancy~~ vacancies and one mole of OH^- ~~vacancy~~ vacancies ~~is~~ are created. Although it is not very clear which of the two defects is the major contributor for electrical conduction at high temperatures for HA, it is obvious that dehydroxylation is an important reaction as far as the generation of these defects is concerned [19] [29]. As ~~the~~ temperature increases, more and more of these defects are generated due to dehydroxylation reaction and when the threshold of these defects concentrations is exceeded, the current flows, leading to the chain reaction and the flash event to occur~~s~~, as discussed earlier [18]. However, it should be kept in mind that the high sintering rates observed in flash sintering can not be explained exclusively by the temperature effect, that is, a higher diffusion rate due to an increase in temperature can not ~~alone~~ explain such high sintering rates by itself[11] [31]~~;~~, therefore, there should be a fundamental change in sintering mechanism causing the observed high sintering rates ~~observed~~.

Referring to figures 5 and ~~figure~~ 6 and to the ~~following~~ reported discussion ~~on it~~, the question that remains to be answered is: what is the reason for the microstructural change to occur which leads to the 'wavy' nature of the conductivity curve, which otherwise should be linear in that temperature range as reported in a previous work [29]?~~.~~ ~~Note~~ One can observe that the conductivity measured up to 1000°C in [29] ~~were~~ corresponds to~~on the~~ dense and porous HA ceramics obtained after sintering at 1300°C; therefore,~~, so~~ it is expected that no microstructural changes ~~happen~~ occur while measuring the conductivity up to 1000°C, ~~giving~~ leading to a the linear increase in conductivity with the temperature.

Liu et al. [30] ~~prepared~~ produced dense (relative density ~~of~~ = 99.8%) HA ceramic ~~by sintering~~ at 925°C by spark plasma sintering technique. Thermal annealing carried out on ~~these~~ such samples at 1000°C and 1100°C revealed a considerable density ~~decrease~~ reduction (~~~~2.5% and ~14% decrease at 1000°C ~~and ~14% decrease~~and ~~at~~ 1100°C, respectively) accompanied with no weight loss. The microstructure of the samples was found to become porous, with ~~the~~ porosity increasing with annealing temperature. The decrease in density (accompanied with no weight loss) and the pores ~~formed~~ formation were attributed to the dehydroxylation reaction (Eq.~~equation~~ 1) which takes place at high temperatures leading to the formation of water vapour. Therefore,~~So~~ according to Liu et al, at the annealing temperature~~s~~, the dehydroxylation reaction leads to pore formation with water vapour being trapped in the closed pores~~,~~ and, as ~~the~~ cooling occurs, rehydration takes place (water enters the lattice) keeping the pores as ~~it is~~they are.

On this basis, ~~We propose the following to~~we can explain the non-linear increase and ~~then~~ successive ~~the~~ decrease of conductivity in the 'wavy' region ~~of the conductivity curve~~as follows. As ~~the~~ temperature increases, more and more water vapour is released due to the dehydroxylation reaction. When the sample achieves sufficient density due to sintering, the conductivity increases; but~~, however~~, at the stage when the sample is dense enough, ~~the~~ closed pores containing water vapour start forming ~~inside~~ within the sample ~~which~~ this causing a~~es~~ conductivity ~~the~~ decrease ~~in conductivity~~. Further density increase ~~in density~~ due to sintering ~~again~~ increases again the conductivity which~~and~~ then decreases due to pores formation, giving the next wave, ~~. T~~this process continuing~~es~~ ~~till~~ until the flash event occurs.

X-ray diffractometry (XRD) analysis

The XRD patterns of as-received powders and sintered samples ~~for both the powder types~~ are shown in figure 8. The ~~patterns of both the powders and all their sintered samples~~peaks account for HA (JCPDS file 09-0432), only, and~~.~~ ~~No~~ no traces of other ~~phases of~~ calcium phosphate~~s~~ phases are observed [17], this indicating that no ~~phase~~ transformation occurred for conventional sintering as well as for flash sintering at all the applied E-fields. These observations are in agreement with previous works on conventional and flash sintering of HA [23] [24] [18]. One can observe that, regardless of the powder type and applied E-field, the sintering is responsible for narrower peaks ~~indicating~~ which point out the formation of well-developed micron-size grains as already shown ~~before~~ in figure 4. The broad peaks for the powders indicate instead that ~~both the powders~~these are poorly crystalline ~~, narrow diffraction peaks for powder would indicate crystalline material which is obtained due to calcination/heat treatment of the powder~~ [24].

(211) diffraction peak is the most prominent for HA. Some diffraction peaks for different sintering conditions show intensities that are not in good agreement with that of standard HA with randomly oriented and grown grains. (002) peak for HA-A sintered ~~at~~ under applied E-field of ~~-~~500 V cm^{-1} is one such peak which show~~s~~~~ing~~ a ~~very large~~certain deviation deviation; the intensity ratio ~~of intensities~~ of (002) and (211) peaks (I_{002}/I_{211}) is seen to be 1.9 ~~which~~ while actually it should be ~0.4 ~~for randomly oriented grains~~ [32]. Such high relative intensity for the (002) peak suggests the (002) preferred orientation and the crystallite c-axis perpendicular to the sample surface [33] [32] [34] [35]. Figure 9 shows the I_{002}/I_{211} for samples sintered at different applied E-field for both the powder types. It can be seen that only HA-A sintered ~~at applied E-field of~~under 500 V cm^{-1} shows (002) preferred orientation. Previous works on flash sintering of HA did not show any such (002) preferred orientation [17] [18]. There are two important differences between ~~the~~ previous and ~~the present~~current study~~.~~~~:~~ 1) In ~~the~~ previous studies, once the flash event occur~~r~~~~s~~~~ed~~, the power supply ~~was~~ is set to switch to current control mode when the current reache~~s~~~~d~~ the pre-set value~~,~~ and the samples ~~were~~ is kept in ~~those~~ such condition~~s~~ for a maximum of 10 s~~econds~~. In the present study, no such pre-set current values were decided; the power setup was turned off manually once the flash event occurred. 2) The maximum sample temperature reached due to the flash event was ~1250°C in previous studies [REF], whereas in ~~this~~ the present work ~~study~~ the maximum furnace temperature for ~~on-set of~~ the flash event is 1317°C ~~which is~~(for HA-A sintered ~~with applied E-field of~~under 500 V cm^{-1}~~.~~). ~~Note~~ It is important to point out that the temperature

Formattato: Evidenziato

reported for ~~this study~~the present study is the furnace temperature and not the sample temperature. The actual temperature of the sample ~~will be~~is definitely higher than 1317°C due to Joule heating which will further rise instantaneously much above during stage II [17] [18]. ~~Coming~~ Going back ~~, referring~~ to figure 5, ~~we~~ one can see ~~that~~that the maximum power dissipation was ~~allowed~~ recorded for HA-A sintered at applied E-filed of 500 V cm^{-1} and~~,~~ ~~a~~ the combination of ~~such~~ high current flow and high temperature (as said, above 1317°C~~, and which will further rise instantaneously~~) can cause partial melting of HA sample [18]. ~~We~~ One speculate that partially melted HA recrystallized with (002) preferred orientation for HA-A sample sintered with applied E-field of 500 V cm^{-1}. Such (002) preferred orientation~~-recrystallization~~ solidification of melted HA ~~giving (002) preferred orientation~~ has been already reported previously [32] [34]. The possible reason for this could be that the C-plane of hexagonal crystal has a closed-packed atomic arrangement and hence C-plane terminated surface is preferred to curtail the surface free energies [35].

FT-IR Analysis

The stability of HA under conventional and flash sintering was ~~also~~ confirmed also by FT-IR analysis. Figure 10 shows IR spectra of as-received powders and samples sintered ~~at~~ under different applied E-fields. As expected, the IR spectra of both ~~the~~ powder types are the same. The sharp bands at around 3570 cm^{-1} correspond to the stretching of isolated OH species that are coordinated in HA. Weak signals at around 1635 cm^{-1} account for the bending of OH species. The broad band between 3000 cm^{-1} and 3700 cm^{-1} observed for both ~~the~~ powders is assigned to physisorbed water molecules~~,~~, ~~and it can be seen that~~ this band weaken~~ings~~ or even disappear~~ings~~ for sintered samples. Strong absorption bands are ~~seen~~ visible below 1500 cm^{-1} ~~which~~ these being ~~are~~ due to asymmetric stretching (γ_3), symmetric stretching (γ_1) and asymmetric bending (γ_4) of PO_4^{-3} unit [35]. The broadening of γ_3 PO_4^{-3} signal for sintered samples compared with that of powder indicates that the structure of PO_4^{-3} is disordered or that oxygen-deficient PO_x ($x \leq 3$) are present in sintered samples [36]. Overall, the IR analysis confirms that regardless of the powder type, HA does not show any type of major structural rearrangement or decomposition upon conventional and flash sintering.

Conclusion

HA ~~with two different powder characteristics were~~was successfully densified by flash sintering starting from with two different powders, considerably reducing the sintering temperature and the processing time. HA is found to be stable ~~for~~ during both conventional ~~as wells as~~and flash sintering conditions, ~~as~~ and no decomposition ~~of HA into other phases~~ is observed, as indicated by XRD and FT-IR analysis. For the samples sintered ~~with a~~under high applied E-field, the conductivity curve ~~for HA~~ is found to be different from that of other materials. At lower temperatures, the conductivity increases constantly with ~~the heating process~~temperature, ~~however~~but, ~~at a temperature~~ above ~850°C the curve~~s~~ show~~s~~ a 'wavy' region. ~~The 'wavy' region in the conductivity curves~~This can be explained by considering the microstructural changes taking place due to the dehydroxylation reaction ~~happening~~ occurring during sintering. The onset temperature for the flash event is found to be different for the two powders ~~types~~ sintered at the same applied E-field. This is because the powder characteristics influence the conductivity curves, although the overall character of the curves remains similar. A combination of high furnace temperature and high current densit~~i~~ves ~~passing through the sample~~ (which will further increase the sample temperature) is shown to cause partial melting of the ~~sample~~material which, ~~. The samples solidified after partial melting~~upon the successive solidification, is shown to ~~possess~~ grow along (002) preferred oriented ~~microstructure~~.

Formattato: Rientro: Prima riga: 1,27 cm, Interlinea: 1,5 righe

References

[1] H. Oonishi, "Orthopaedic applications of hydroxyapatite," *Biomaterials,* vol. 12, pp. 171-178, 1991.

[2] Z. Zyman, V. Glushko, V. Filippenko, V. Radchenko and V. Mezentsev, "Nonstoichiometric hydroxyapatite granules for orthopaedic applications," *Journal of Materials Science: Materials in Medicine,* vol. 15, p. 551–558, 2004.

[3] C. Schwartz, P. Lecestre, P. Frayssinet and P. Liss, "Orthopaedic Surgery & Bone substitutes," p. 161–165, 1999.

[4] S. J. Kalita, A. Bhardwaj and H. Bhatt, "Nanocrystalline calcium phosphate ceramics in biomedical engineering," *Materials Science and Engineering: C,* vol. 27, p. 441–449, 2007.

[5] M. Fanovich, M. Castro and J. P. Lopez, "Analysis of the microstructural evolution in hydroxyapatite ceramics by electrical characterisation," *Ceramics International,* vol. 25, p. 517–522, 1999.

[6] W. Suchanek, M. Yashima, M. Kakihana and M. Yoshimura, "Hydroxyapatite ceramics with selected sintering additives," *Biomaterials,* vol. 18, p. 923–933, 1997.

[7] S. Raynaud, E. Champion, J. P. Lafon and Bernache-Assollan, "Calcium phosphate apatites with variable Ca/P atomic ratio III. Mechanical properties and degradation in solution of hot pressed ceramics," *Biomaterials,* vol. 23, p. 1081–1089, 2002.

[8] D. Veljović, B. Jokić, R. Petrović, E. Palcevskis, Dindune, I. N. Mihailescu and et al, "Processing of dense nanostructured HAP ceramics by sintering and hot pressing," *Ceramics International,* vol. 35, p. 1407–1413, 2009.

[9] F. Wakai, Y. Kodama, S. Sakaguchi and T. Nonami, "Superplasticity of Hot Isostatically Pressed Hydroxyapatite," *Journal of American Ceramic Society,* vol. 73, p. 457–460, 1990.

[10] M. Cologna, B. Rashkova and R. Raj, "Flash Sintering of Nanograin Zirconia in <5 s at 850°C," *Journal of American Ceramic Society,* vol. 93, pp. 3556-3559, 2010.

[11] R. Raj, "Joule heating during flash-sintering.," *Journal of European Ceramic Society,* vol. 32, pp. 2293-2301, 2012.

[12] M. Biesuz and V. M. Sglavo, "Flash sintering of alumina: effect of different operating conditions on densification," *Journal of European Ceramic Society,* vol. 36, p. 2535–2542, 2016.

[13] J. Luo, "The scientific questions and technological opportunities of flash sintering: from a case study of ZnO to other ceramics," *Scripta Materialia,* vol. 146, pp. 260-266, 2018.

[14] S. K. Jha and R. Raj, "The effect of electric field on sintering and electrical conductivity of Titania," *Journal of American Ceramic Society,* vol. 97, pp. 527-534, 2014.

[15] A. Karakuscu, M. Cologna, D. Yarotski, J. Won, J. S. Francis, R. Raj and B. P. Uberuaga, "Defect structure of flash-sintered strontium titanate," *Journal of American Ceramic Society,* vol. 95, p. 2531–2536, 2012.

[16] A. L. Prette, M. Cologna, V. M. Sglavo and R. Raj, "Flash-sintering of Co2MnO4 spinel for solid oxide fuel cell applications," *Journal of Power Sources,* vol. 196, pp. 2061-2065, 2011.

[17] I. R. Lavagnini, J. V. Campos, A. G. Storion, A. D. Lobo, R. Raj and E. M. Pallone, "Influence of flash sintering on phase transformation and conductivity of hydroxyapatite," *Ceramics International,* vol. 47, no. 7, pp. 9125-9131, 2021.

[18] C. Hwang and J. Yun, "Flash sintering of hydroxyapatite ceramics," *Journal of Asian Ceramic Society,* vol. 1, no. 9, pp. 304-311, 2021.

[19] B. I, Y. H. Han, J. Yun, J. Francis, S. Kim and R. Raj, "Preliminary investigation of hydroxyapatite microstructures prepared by flash sintering," *Advances in Applied Ceramics,* vol. 115, no. 5, pp. 276-281, 2016.

[20] J. S. Francis, M. Cologna and R. Raj, "Particle size Effects in Flash Sintering," *Journal of European Ceramic Society,* vol. 32, pp. 3129-3136, 2012.

[21] M. Cologna, J. S. Francis and R. Raj, "Field assisted and flash sintering of alumina and its relationship to conductivity and MgO-doping," *Journal of European Ceramic Society,* vol. 31, pp. 2827-2837, 2011.

[22] K. S. Naik, V. M. Sglavo and R. Raj, "Field assisted sintering of ceramic constituted by alumina and yttria stabilized zirconia," *Journal of European Ceramic Society,* vol. 34, pp. 2435-2442, 2014.

[23] N. Thangamania, K. Chinnakalib and F. D. Gnanam, "The effect of powder processing on densification, microstructure and mechanical properties of hydroxyapatite," *Ceramics International,* vol. 28, p. 355–362, 2002.

[24] I. R. GIBSON, S. KE, S. M. BEST and W. BONFIELD, "Effect of powder characteristics on the sinterability of hydroxyapatite powders," *JOURNAL OF MATER IALS SCIENCE: MATER IALS IN MEDICINE,* vol. 12, pp. 163-171, 2001.

[25] J. Francis and R. Raj, "Influence of the Field and the Current Limit on Flash Sintering at Isothermal Furnace Temperatures," *Journal of American Ceramic Society,* vol. 96, pp. 2754-2758, 2013.

[26] K. Yamashita, K. Kitagaki and T. Umegaki, "Thermal instability and proton conductivity of ceramic hydroxyapatite at high temperatures," *Journal of American Ceramic Society,* vol. 78, pp. 1191-1197, 1995.

[27] K. Yamashita, H. Owada, H. Nakagawa and et al, "Trivalent-cation-substituted calcium oxyhydroxyapatite," *Journal of American Ceramic Society,* Vols. 590-594, p. 69, 1986.

[28] T. Takahashi, S. Tanase and O. Yamamoto, "Electrical conductivity of some hydroxyapatites," *Electrochimica Acta,* vol. 23, pp. 369-373, 1978.

[29] J. P. Gittings, C. R. Bowen, A. C. Dent and et al, "Electrical characterization of hydroxyapatite-based bioceramics," *Acta Biomaterialia,* vol. 5, pp. 743-754, 2009.

[30] Y. Liu and Z. Shen, "Dehydroxylation of hydroxyapatite in dense bulk ceramics sintered by spark plasma sintering," *Journal of European Ceramic Society,* vol. 32, pp. 2691-2696, 2012.

[31] W. Qin, H. Majidi, J. Yun and et al, "Electrode effects on microstructure formation during FLASH sintering of yttrium-stabilized zirconia," *Journal of American Ceramic Society,* vol. 99, pp. 2253-2259, 2016.

[32] C. M. Roome and C. D. Adam, "Crystallite orientation and anisotropic strains in thermally sprayed hydroxyapatite coatings," *Biomaterials,* vol. 16, pp. 691-696, 1995.

[33] D. Grossin, S. Rollin-Martinet, C. Estournès, F. Rossignol, E. Champion, C. Combes, C. Rey, C. Geoffroy and C. Drouet, "Biomimetic apatite sintered at very low temperature by spark plasma sintering: Physico-chemistry and microstructure aspects," *Acta Biomaterialia,* vol. 6, pp. 577-585, 2010.

[34] X. Liu, D. He, Z. Zhou, G. Wang, Z. Wang, X. Wu and Z. Tan, "Characteristics of (002) Oriented Hydroxyapatite Coatings Deposited by Atmospheric Plasma Spraying," *Coatings,* vol. 8, p. 258, 2018.

[35] H. Akazawa and Y. Ueno, "Growth of preferentially c-axis oriented hydroxyapatite thin films on Si(1 0 0) substrate by electron-cyclotron-resonance plasma sputtering," *Applied Surface Science,* vol. 276, pp. 217-222, 2013.

[36] M. Hamdi and A. Ide-Ektessabi, "Preparation of hydroxyapatite layer by ion beam assisted simultaneous vapor deposition," *Surface and Coating Technology,* Vols. 163-164, pp. 362-367, 2003.

Tables

Electric field ($V\ cm^{-1}$)		0	500	1000	1500	2000
Relative density (%)	HA-A	96	94	93	95	92
	HA-B	91	93	90	90	95

Table 1. Final density of samples sintered at different applied E-field for HA-A and HA-B

Figures

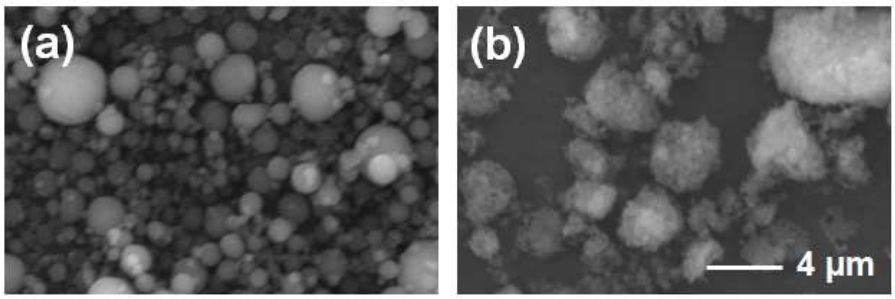

Figure 1. Micrographs of (a) HA-A and (b) HA-B powders.

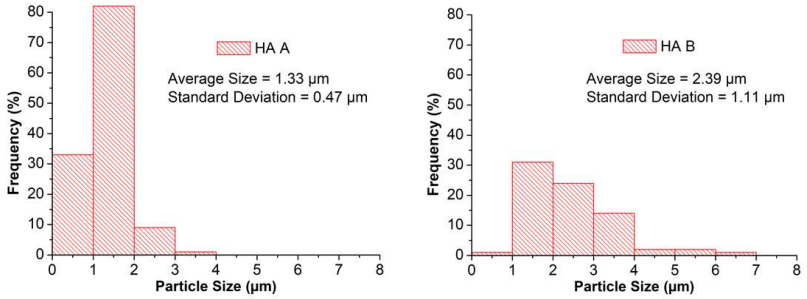

Figure 2. Particle size distribution for HA-A and HA-B powders.

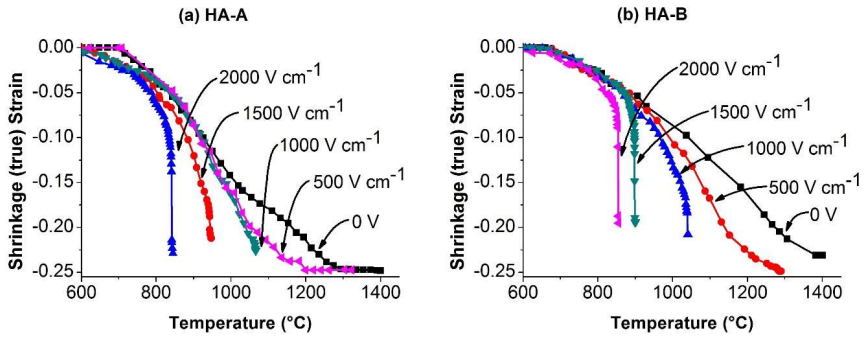

Figure 3. Shrinkage strain as a function of furnace temperature at different applied E-fields for (a) HA-A and (b) HA-B.

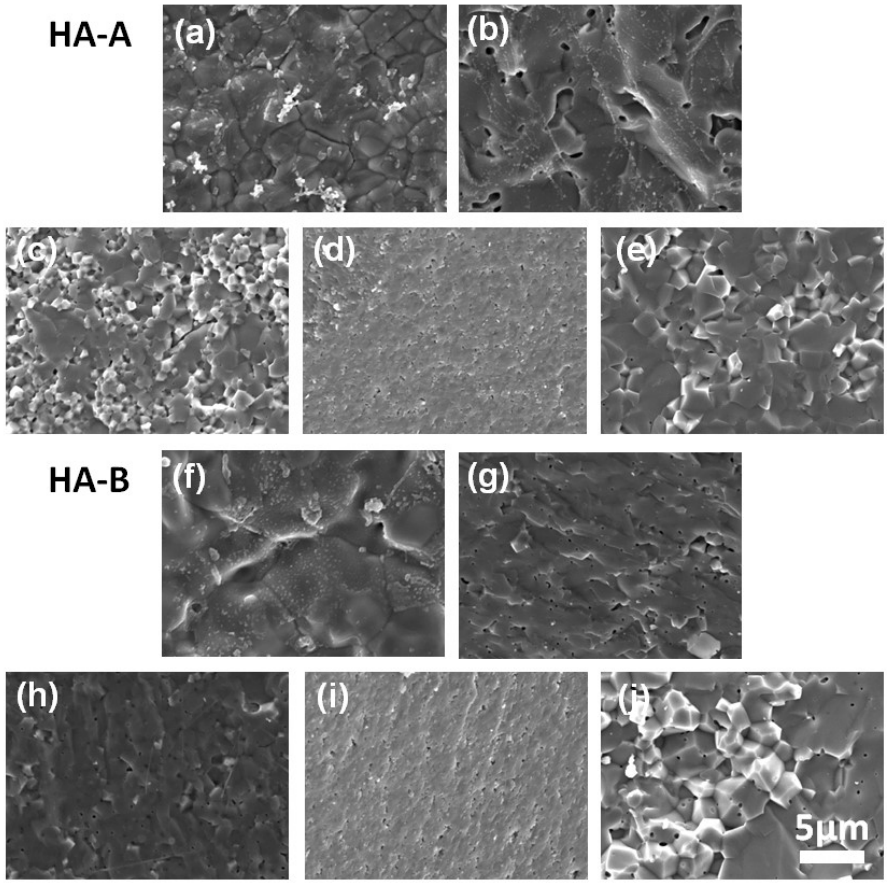

Figure 4. Microstructures of HA-A sintered at (a-e) 0-2000 Vcm^{-1} and of HA-B sintered at (f-j) 0-2000 V cm^{-1} applied E-field.

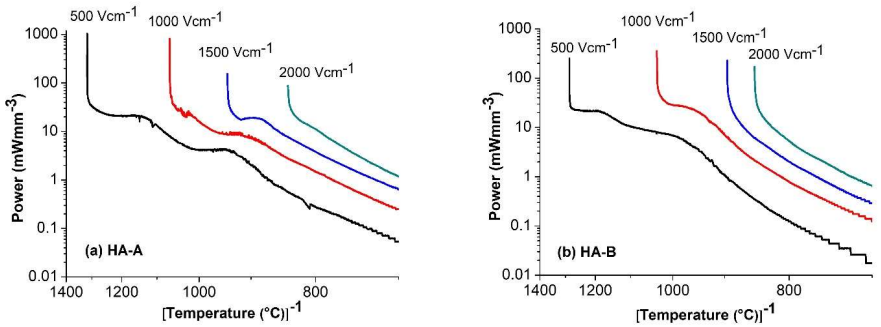

Figure 5. Arrhenius plots of power density of flash sintered samples under different applied E-fields for (a) HA-A and (b) HA-B.

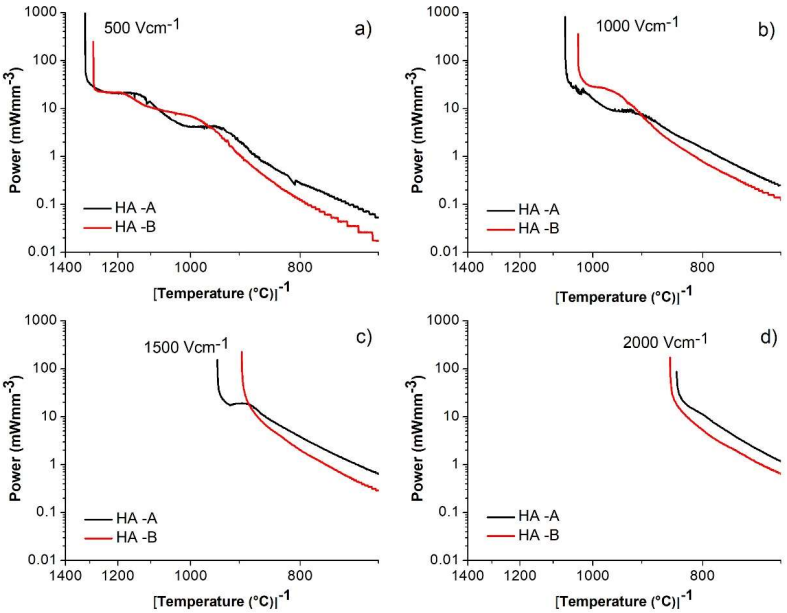

Figure 6. Arrhenius plot of power density for HA-A and HA-B flash sintered at applied E-field of (a) 500 V cm^{-1} (b) 1000 V cm^{-1} (c) 1500 V cm^{-1} (d) 2000 V cm^{-1}.

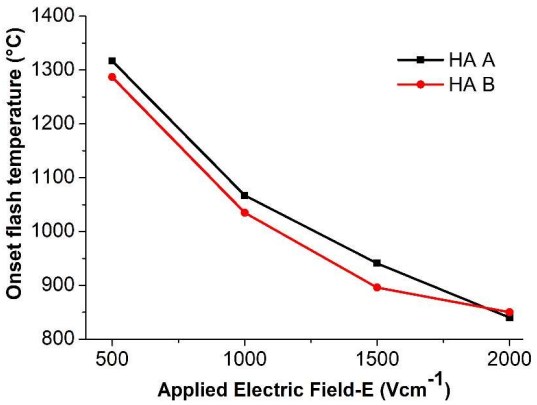

Figure 7. Temperature for onset of flash for different applied E-field for HA-A and HA-B.

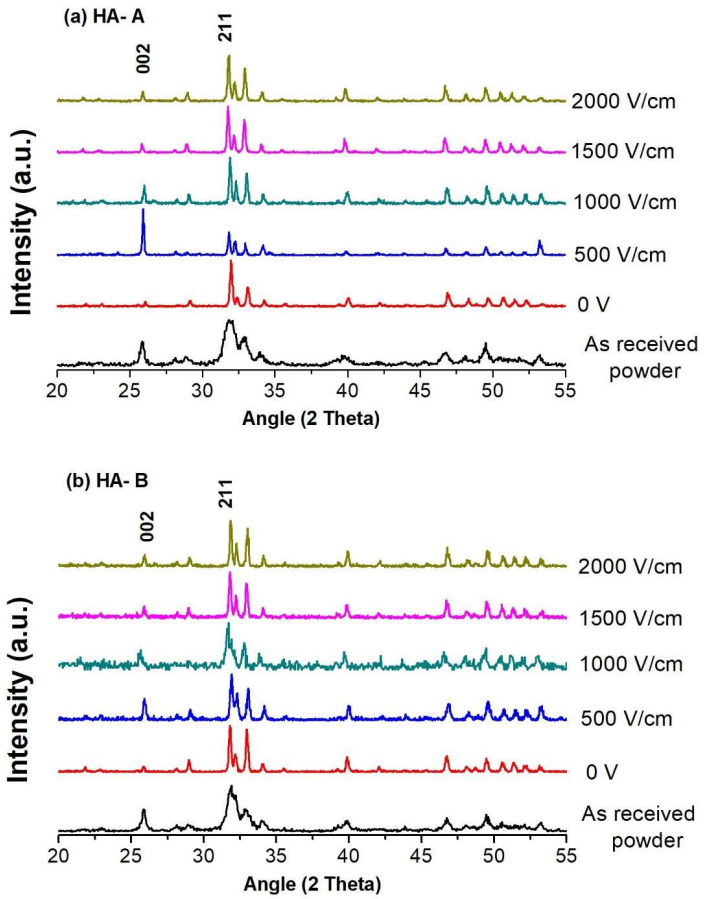

Figure 8. XRD spectra of as received powders and samples sintered at different applied E-field for (a)HA-A and (b) HA-B.

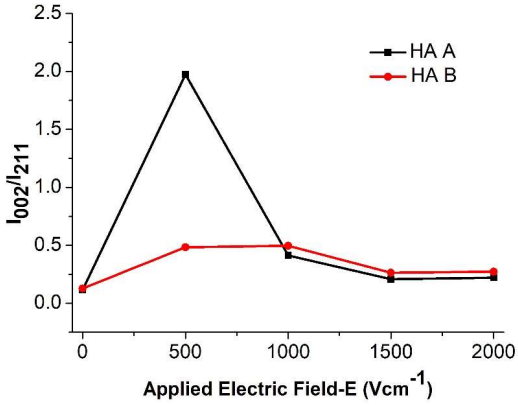

Figure 9. I_{002}/I_{211} for samples sintered at different applied E-field for HA-A and HA-B.

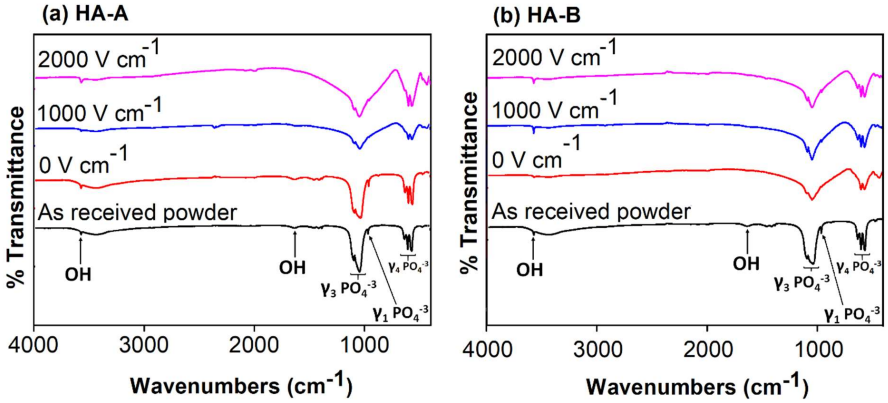

Figure 10. Infrared spectra of (a) HA-A and (b) HA-B at different applied E-fields.